LANGMUIR

Article

pubs.acs.org/Langmuir

Effects of Confinement on the Dielectric Response of Water Extends up to Mesoscale Dimensions

Sergio De Luca,[*,†,‡] Sridhar Kumar Kannam,[∥] B. D. Todd,[‡,§] Federico Frascoli,[‡,§] J. S. Hansen,[⊥] and Peter J. Daivis[#]

[†]School of Chemical Engineering, Integrated Material Design Centre (IMDC), University of New South Wales, Sydney, NSW 2033, Australia

[‡]Department of Mathematics, Faculty of Science, Engineering and Technology, and [§]Centre for Molecular Simulation, Swinburne University of Technology, Melbourne, Victoria 3122, Australia

[∥]IBM Research Australia, 204 Lygon Street, Carlton, Victoria 3053, Australia

[⊥]DNRF Center "Glass and Time", IMFUFA, Department of Science and Environment, Roskilde University, DK-4000 Roskilde, Denmark

[#]School of Applied Sciences, RMIT University, Melbourne, Victoria 3001, Australia

ABSTRACT: The extent of confinement effects on water is not clear in the literature. While some properties are affected only within a few nanometers from the wall surface, others are affected over long length scales, but the range is not clear. In this work, we have examined the dielectric response of confined water under the influence of external electric fields along with the dipolar fluctuations at equilibrium. The confinement induces a strong anisotropic effect which is evident up to 100 nm channel width, and may extend to macroscopic dimensions. The root-mean-square fluctuations of the total orientational dipole moment in the direction perpendicular to the surfaces is 1 order of magnitude smaller than the value attained in the parallel direction and is independent of the channel width. Consequently, the isotropic condition is unlikely to be recovered until the channel width reaches macroscopic dimensions. Consistent with dipole moment fluctuations, the effect of confinement on the dielectric response also persists up to channel widths considerably beyond 100 nm. When an electric field is applied in the perpendicular direction, the orientational relaxation is 3 orders of magnitude faster than the dipolar relaxation in the parallel direction and independent of temperature.

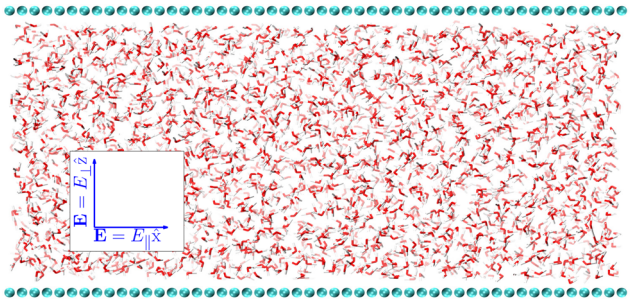

INTRODUCTION

Experimental and computer simulation studies on confined fluid systems suggest that interfacial effects extend only to a few nanometers from the interface,[1,2] while others have found long-range surface induced structuring effects.[3,4] X-ray scattering measurements near surfaces reveal a density increase in interfacial water compared to bulk water,[5] and X-ray diffraction shows layering effects in the first hydration layers.[6] Interfaces also affect the orientational dynamics of water reducing the dielectric relaxation time, as observed by terahertz time-domain spectroscopy.[7] Relaxation dynamics becomes strongly anisotropic in a confined environment, such as between graphene surfaces,[8] where the faster relaxation is evinced for the confined direction. von Domaros et al.[9] examined the dipole orientational relaxation of confined water at the wall's interface and found an order of magnitude difference due to the difference in orientation of water at the upper and lower walls.

Confinement affects coexistence properties of fluids. The fluid critical density and critical temperature approach bulk values at large slit pore width (40 molecular diameters).[10] Vapor−liquid interfacial properties also dramatically change under confinement, such as the phase coexistence liquid−vapor surface tension and is reduced many fold under confinement.[11] Investigations of the shift in critical temperature and density and of the coexistence densities as a function of the slit pore width demonstrated that these properties are general properties of confined fluids.[12]

Confinement affects water's static and dynamic properties,[13] further unfolding a variety of intriguing phenomena when hydrodynamics couples with electrostatics, such as electro-pumping,[14−18] electromelting,[19] and electrostriction.[20] These phenomena are rooted in the complicated interplay between hydrogen bond network strength, interface induced orientation effects and the dipole alignment due to the electric field injected torque. An external electric field influences thermo-physical fluid properties. The vapor−liquid coexistence curve

Received: March 2, 2016
Revised: April 21, 2016
Published: April 26, 2016

DOI: 10.1021/acs.langmuir.6b00791
Langmuir 2016, 32, 4765−4773

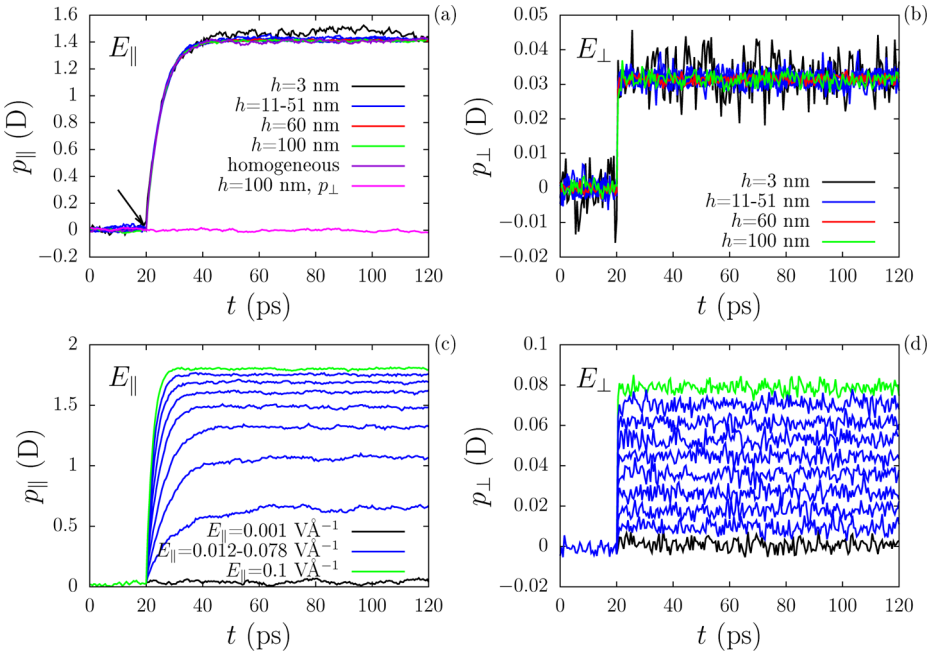

Figure 1. Polarization of confined water with time. The arrow in (a) indicates the time when the electric field is switched on. An external field E = 0.04 VÅ^{-1} is applied in (a) parallel and (b) perpendicular directions for different channel widths. (c) and (d) are for a fixed channel width h = 11 nm and varying electric field.

shows a decrease of the critical temperature of confined water and a decrease of the saturated liquid phase density.[21]

In linear, homogeneous, and isotropic systems the dielectric constant of water ϵ is a scalar quantity[22] which can be measured via linear response theory by monitoring the dipole moment fluctuations[22,23] or via nonequilibrium molecular dynamics (NEMD) applying a static field[24−27] and tracking the polarization response. When a spatially varying electric field is applied the dielectric response of water becomes wave vector dependent.[28]

In confined geometries, the dielectric response is anisotropic and ϵ becomes a second-rank tensor whose elements are dependent on spatial coordinates if the medium is inhomogeneous,[29−31] such as close to an interface. An overscreening behavior[27,30,31] manifests in the perpendicular direction, i.e., $\epsilon_\perp < \epsilon_\parallel$ for nanoscopic systems. Similarly, atomic force microscopy experiments on interfacial water reveal $\epsilon \sim 4$, reaching the bulk value $\epsilon \sim 80$ approximately 10 nm away from a solid interface.[32] Thin film water measurements[33,34] with gap widths from micrometer to nanoscale dimensions show $\epsilon_\perp \lesssim 10$, consistent with recent results from dielectric property measurements of guest water molecules inserted in porous metal−organic crystals.[35]

Despite the large amount of knowledge gathered, it is still not fully understood if the effects on the total dipole moment behavior of the fluid system are short or long ranged. The main result of this work is the finding that the *fluctuations* of the total dipole moment of water are affected by the confinement potentially up to macroscopic dimensions. In particular, we find that when liquid water is confined between two planar solid surfaces the root-mean-square fluctuations (rms) of the perpendicular component of the total dipole moment of water is 1 order of magnitude smaller than the bulk fluctuations and constant for channel widths at least as large as 100 nm. This strong anisotropy in the dynamics of the orientational polarization extends out to at least mesoscale dimensions, and possibly out to macroscopic length scales. By applying a spatially uniform and static electric field in the perpendicular direction we find that the dipole alignment is very fast and resembles a step function, contrary to the typical exponential shape of the dielectric relaxation observed in homogeneous systems or when the field is applied parallel to the surfaces.

The next section summarizes the molecular dynamic simulation methods, and a detailed dielectric characterization of our fluid system is provided in the Results section. This is required to compare the dipole moment in the parallel and perpendicular directions for the same local electric field (and not the external field) and to establish the reliability of the dipole moment signal.

METHODS

Two planar uncharged hydrophobic graphene-like surfaces enclose SPC/E model water molecules (constrained with SHAKE) with a permanent dipole moment of 2.35 D in agreement with the experimental value 2.9 ± 0.6 D.[36] The van der Waals interaction parameters between water molecules and carbon atoms of the graphene (ϵ = 0.09369 kcal/mol, σ = 3.19 Å) are taken from Werder et al.[37] which are shown to reproduce the experimental contact angles of water on graphene surface. Walls lie in the $x - y$ periodic plane and z is the perpendicular or confined direction. Quantum, liquid-surface chemical reactions (thus any charge transfer mechanism) and atomic and electronic polarizability effects are neglected. We use a rigid and nonpolarizable water model because our study only pertains to the orientational polarization mechanism. The nonpolarizable SPC/E water model has been demonstrated to be appropriate to model water in the presence of strong electric fields.[38] Future investigations will be carried out using polarizable models of water.[39] The system is equilibrated for 3 ns with a time step of 1 fs, before data collection is performed for 1 ns. The short-range repulsive part and the dipole-induced attractive part of the interaction between particles is modeled through the pairwise additive LJ potential with a cutoff length of 1 nm.[15] The long-range electrostatic interactions are modeled employing the Ewald algorithm adapted for slab geometry as implemented in LAMMPS[40,41] with a cutoff truncation radius of 1 nm and with

DOI: 10.1021/acs.langmuir.6b00791
Langmuir 2016, 32, 4765−4773

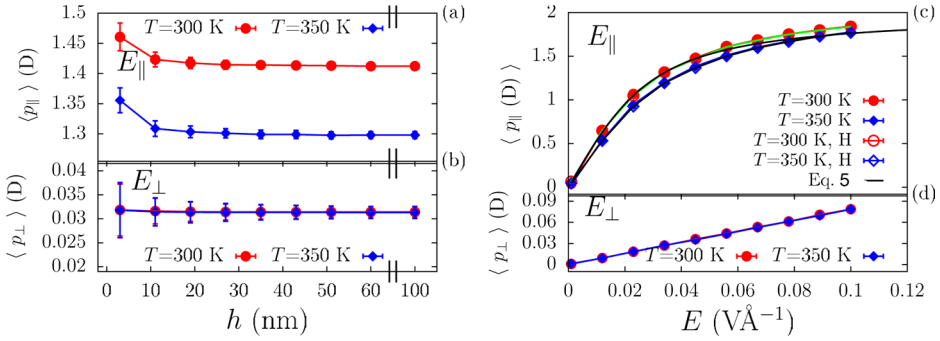

Figure 2. Polarization of confined water with the channel width when the field E = 0.04 VÅ^{-1} is applied in (a) parallel and (b) perpendicular directions. Polarization of confined water with the external field applied in (c) parallel and (d) perpendicular directions, for a channel of width h = 11 nm. Black lines are the Langevin equation, eq 2. H indicates the homogeneous system, and the angle brackets indicate the new equilibrium state time averages. The error bars in (c) and (d) are smaller than symbol sizes.

specified accuracy in forces[41] of 10^{-5}. Periodic tinfoil (conducting metal) boundary conditions are applied in the x and y directions. Vacuum boundary conditions are applied in the z direction for the Ewald algorithm, with the slab geometry correction[40] in which an empty volume is inserted such that the extended confined dimension is three times the actual channel size.[40,41] The corrected Ewald algorithm is also named EW3DC.[40] Note that every system examined in this study is electroneutral, making the EW3DC choice appropriate. For confined systems carrying a net charge, a neutralization procedure based on a background-charge correction must be implemented[42,43] to avoid spurious electrostatic potentials across the channel. The bulk density of water is fixed at ρ = 998 kg m^{-3}, and the procedure to estimate its accessible volume for the graphene channels is described in ref.[15] The simulations are carried out in the NVT ensemble with the Nosé−Hoover thermostat using the MD software package LAMMPS.[41] Due to the incompressibility of liquid water, small variations in the fluid density may cause strong variations in the fluid pressure when the system volume is fixed. To verify that our results do not depend on small density variations we performed equilibrium simulations in the NPT ensemble with the nanochannel h = 11 nm immersed in a larger water reservoir of 10 × 10 × 15 nm^3 and setting the barostat at 1.01 bar. The density of water inside the channel has been obtained considering the same volume as the NVT systems. We found 2.6% lower density inside the nanochannels compared to the fixed density ρ = 998 kg m^{-3} we have used in the simulations with an applied field. We have verified that this small difference in the density of water has no detectable effect on the property measurements reported in this paper. Note that although the thermostat acts on the fluid and not the walls, this is justified because no flow occurs. Bernardi et al.[44] have previously shown that serious side effects can occur for thermostated confined fluids under flow conditions, but under zero flow conditions there are no significant artifacts. Notwithstanding, we verified that using a Langevin thermostat, in conjunction with the TIP3P water model, gives the same results suggesting that this effect is not a peculiarity of any specific water model or thermostatting strategy. Surfaces are kept rigid during the simulations and assumed electrically transparent for simplicity. The simulation box dimensions in x and y for the graphene channel are L_x = 6.02 nm, L_y = 6.24 nm. Channel widths (z-direction) range from h = 3 nm to h = 100 nm. The range of applied electric field amplitudes used in this work are smaller or comparable to previous molecular dynamics studies of confined water subjected to an external static electric field, such as E = 3.0 VÅ^{-1} applied to water confined between Pt(111) walls[38] and E = 0.2 VÅ^{-1} applied to water confined between graphite and mica pores,[21] and is approximately 2 orders of magnitude higher than experiment.[45] For some systems, five independent simulations with different initial velocity distributions are carried out to verify the reproducibility of the results and to estimate the statistical errors. After the application of the external electric field, each independent simulation yields almost exactly the same average dipole moment and the same statistical error, suggesting the achievement of an appropriate new equilibrium state.

RESULTS

We denote by $\mathbf{M} = \sum_{i=1}^{N_w} \boldsymbol{\mu}_i$ the total liquid dipole moment where $\boldsymbol{\mu}_i$ is the dipole moment of a single molecule and N_w is the total number of water molecules. In Figure 1 we show the dielectric response of the system with the field applied along the parallel and perpendicular directions to the walls, varying the graphene channel width. Figure 1a plots the time-series of the x-component of the average net dipole moment of water $p_x(t) = p_\parallel(t) = \mathrm{M}_\parallel(t)/N_w = \sum_{i=1}^{N_w} \mu_{\parallel,i}(t)/N_w$ where $\mu_{\parallel,i}$ is the projection of the dipole moment $\boldsymbol{\mu}_i$ in the parallel x−direction and $\mathrm{M}_\parallel$ is the projection of $\mathbf{M}$ in the same direction. The system is subjected to a static and spatially uniform electric field polarized in the parallel x−direction i.e., $\mathbf{E}_\parallel = E_\parallel \hat{\mathbf{x}}$ with fixed amplitude $E_\parallel = E$ = 0.04 VÅ^{-1} switched on at t = 20 ps. Samples are taken every 500 fs. We also plot $p_\parallel(t)$ for the homogeneous system (with no walls) having approximately the same lateral box sizes as the confined system with h = 11 nm. It can be seen that the dielectric response of the confined system is equal to the homogeneous system response, both yielding in the new equilibrium state (after the field is applied and the polarization signal is stable) $p_x \simeq$1.4 D (after $t \sim$ 60 ps). As expected, $p_\parallel$ does not depend on h since the applied electric field is constant and equal for every system. However, the fluctuations depend on the channel width, are affected by the presence of the electric field, and strongly depend on the direction. For both the intervals 0−20 ps ($E_\parallel$ = 0) and 20−120 ps ($E_\parallel \neq 0$) the fluctuations are similar for every h except for the channel width 3 nm, where the closer surfaces perturb water significantly.

We monitor $p_\perp$ applying $\mathbf{E}_\perp = E_\perp \hat{\mathbf{z}}$ with $E_\perp$ = 0.04 VÅ^{-1} plotted in Figure 1b (same external field as before). The fluctuations of the signal $p_\perp(t)$ are much smaller compared to the parallel case, for both the $E_\perp$ = 0 case (0−20 ps) and the $E_\perp \neq 0$ case (20−120 ps). This signal has also been plotted in Figure 1a for comparison (pink line). Moreover, the transient part of the signal $p_\perp(t)$, i.e., immediately after the application of the electric field, has a completely different shape compared to the classical Debye-like exponential dielectric relaxation observed in the parallel case (Figure 1a). We will show that the effect is unaltered when the *local* field, i.e., the sum of the external field and the induced field, for both the directions is equal. We will exclude any nonlinear effect showing that when the external field is $E_\perp \lesssim$ 0.02 VÅ^{-1} we are in the linear regime as discussed below (comparing with the Langevin function[26]).

For h = 11 nm and the field $\mathbf{E} = E_\parallel \hat{\mathbf{x}}$ with varying the electric field amplitudes in the interval 0.001−0.1 VÅ^{-1} gives the time series plotted in Figure 1c. As expected, $p_\parallel$ monotonically

DOI: 10.1021/acs.langmuir.6b00791
Langmuir 2016, 32, 4765−4773

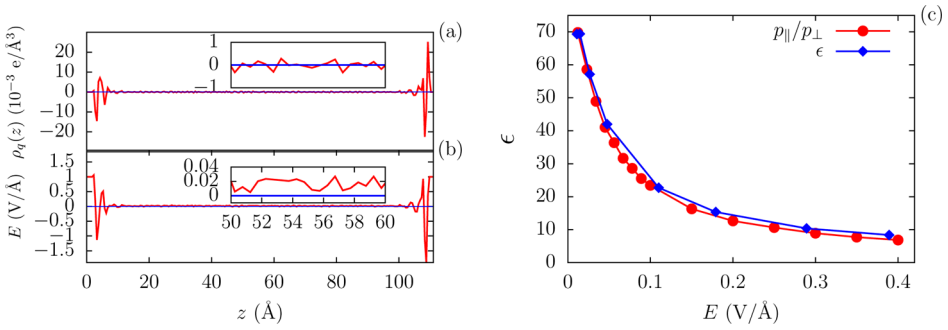

Figure 3. (a) Charge density and (b) local electric field profiles of confined water for h = 11 nm and E_0 = 1 VÅ^{-1}. Insets show the close view at the center of the channel. (c) Dielectric constant (ϵ) of water with electric field calculated using eq 5.

increases at increasing amplitudes, since the dipole alignment depends on the torque exerted on the dipoles $\boldsymbol{\Gamma}_i = \boldsymbol{\mu}_i \times \mathbf{E}$ which increases as the field increases. For $E_\parallel$ = 0.001 VÅ^{-1} no response is detected within statistical uncertainty (black profile) since the thermally induced noise amplitude is larger than the dipole response. The highest field, E = 0.1 VÅ^{-1} (green line), yields the largest dipolar response ~1.7 D. Figure 1d plots $p_\perp(t)$ applying $\mathbf{E} = E_\perp\hat{\mathbf{z}}$. A strong reduction of the dipole moment due to the depolarizing field originating from the dipole surface charge density at the interfaces is observed. Moreover, the relaxation time is an order of magnitude faster. These aspects will be discussed later on.

Figure 2a shows the new equilibrium state average values of the signals $p_\parallel(t)$ plotted in Figure 1a as a function of pore width, denoted with $\langle p_\parallel(t)\rangle$. Standard errors are computed for 120 independent samples separated by 500 fs. Apart from the h = 3 nm case, where the details of the solid/liquid interface begin to be significant due to the high surface-to-volume ratio, $\langle p_\parallel(t)\rangle$ does not depend on h, as expected. However, at T = 350 K the increased thermal energy competes against the alignment effect of the torque exerted by the electric field on the dipoles randomizing the orientations, thus substantially lowering $\langle p_\parallel(t)\rangle$ at T = 350 K.

Figure 2b reports the averages $\langle p_\perp(t)\rangle$ plotted in Figure 1b. It can be seen that the standard errors are smaller compared to the parallel direction (note the smaller scale on y-axis in the perpendicular direction). Interestingly, contrary to the parallel case, $\langle p_\perp\rangle$ does *not* depend on the temperature, at least in the temperature range examined in this work. In the linear regime, $\mathbf{p}_\perp = \alpha_\perp\mathbf{E}_\perp$ (to be shown later), where $\mathbf{p}_\perp$ is the average dipole moment in the perpendicular direction, $\mathbf{E}_\perp$ is the local electric field, and $\alpha_\perp$ is the polarizability.[46] To a first approximation,[47] we then have the permittivity

$$\epsilon = 1 + \rho\alpha/\epsilon_0 \tag{1}$$

where ρ is the density of water and $\epsilon_0 = 8.854 \times 10^{-12}$ F m^{-1} is the vacuum permittivity. From this we can conclude that if α is constant and does not depend on T, then also ϵ is constant and does not depend on T, in qualitative agreement with a recent experiment performed above room temperature.[35]

New equilibrium state averages taken from profiles of Figure 1c obtained applying the fields $\mathbf{E} = E_\parallel\hat{\mathbf{x}}$ are plotted in Figure 2c with red filled circles. We also plot data for the homogeneous system (empty red circles), for the confined system at T = 350 K, and for the homogeneous system at T = 350 K. Up to field strengths around ≈0.02 VÅ^{-1}, the polarization response is approximately linear, in accord with literature,[24,26] whereas saturation effects begin to take place for $E \gtrsim 0.04$ VÅ^{-1}. We note also that the homogeneous system dielectric response *exactly* corresponds to the dielectric response of the confined system in the parallel direction. As noted earlier, the increased thermal energy of the fluid at T = 350 K increases the randomization of the permanent dipole moment orientations, decreasing $\langle p_\parallel\rangle$ at T = 350 K compared to the T = 300 K measurements. This is true for both the confined and homogeneous system.

The polarization response of water at high fields deviates from linearity and nonlinearities are captured by the Langevin function which has been derived considering the orientational polarization of systems composed of noninteracting dipoles. The Langevin function is[25,26,46]

$$p(E) = A\left(\coth(BE) - \frac{1}{BE}\right) \tag{2}$$

plotted in Figure 2c with fitting parameters A = 2 D and B = 83.7 Å V^{-1} for T = 300 K and E being the local electric field, which in the parallel direction is usually assumed to coincide with the external field. Figure 2c shows that when the external field is $E_\parallel \approx 0.02$ VÅ $^{-1}$, we are in the linear regime. We emphasize at this point that a static electric field does not perform any macroscopic thermodynamic work on the fluid system, even though there are microscopic fluctuations of the total dipole moment. Hence, there are no heating effects to be considered in our case, such as when a microwave field[48,49] is applied. A small amount of work is performed only during the transient time in which the dipoles align with the field, and the heat generated is absorbed by the thermostat. Averaging in the perpendicular direction, i.e., averaging $p_\perp(t)$ from Figure 1d taken in the new equilibrium state, leads to the results plotted in Figure 2d which illustrates that the linear regime is attained. In the perpendicular direction, the effect of the higher thermal energy is almost undetectable.

As mentioned above, Figure 1d plots $p_\perp(t)$ applying $\mathbf{E} = E_\perp\hat{\mathbf{z}}$. The depolarizing (induced) field, i.e., the electric field due to the polarization of the water molecules, screens the external field, causing $\langle p_\perp\rangle \ll \langle p_\parallel\rangle$. For any field, the fluctuation amplitudes are visibly smaller than the fluctuation amplitudes of the parallel case (Figure 1c), considering the much smaller scale of the y-axis in the perpendicular case. In homogeneous systems and in the direction parallel to the walls, the local electric field can be approximated with the external field.[38] In the perpendicular direction, for a system periodic in the directions x and y and confined along z, the electric field E_p due to the polarization of water in response to the external field E_0 applied across z is[38]

DOI: 10.1021/acs.langmuir.6b00791
Langmuir 2016, 32, 4765−4773

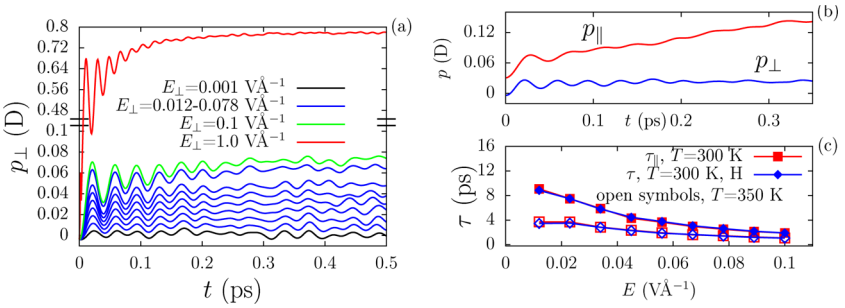

Figure 4. (a) Dipole moment over a short time after the field is switched on in the perpendicular direction, same as Figure 1d. (b) $p_\perp$ and $p_\parallel$ with the time at an external field E = 0.034 VÅ^{-1}. (c) Dielectric relaxation time with the external field. Channel width h = 11 nm. H indicates the homogeneous system.

$$E_p(z) = \frac{\int_0^z \rho_q(z')\,dz'}{\epsilon_0} \tag{3}$$

where $\rho_q(z')$ is the charge density distribution and ϵ_0 is the vacuum permittivity. The total electric field is[38]

$$E(z) = E_0 + E_p(z) \tag{4}$$

which allows us to estimate the dielectric constant ϵ of water at a specific electric field[38]

$$\epsilon = \frac{E_0}{E} \tag{5}$$

When the external field is E_0 = 1 V Å^{-1}, the local field, eq 4, gives in the center of the channel E = 0.015 V Å^{-1}. This can be observed in Figure 3a for $\rho_q(z)$ and in part (b) for $E(z)$, yielding $\epsilon_\perp = E_0/E = 68 \pm 10$, in agreement with earlier studies.[38] Figure 3c plots the field-dependent dielectric constant of water, compared with the new equilibrium state values of $p_\parallel/p_\perp$ computed for the same applied fields. The agreement could be explained by noting that $p = \epsilon_0(\epsilon - 1)E$ assuming $\epsilon_\perp = \epsilon_\parallel = \epsilon$, where E is the local field and $E_\parallel/E_\perp = E_0/E = \epsilon$. This explains why in the external field range examined the polarization shows nonlinearities in the parallel direction (Figure 2c), whereas in the perpendicular directions we are still in the linear regime (Figure 2d).

Figure 4a shows the average dipole moment per molecule $p_\perp$ at varying external electric fields taken from Figure 1d for short times. The signal is observed for the first 500 fs after the field is switched on and is sampled every femtosecond. For the external field $E_\perp$ = 1 VÅ^{-1} (we will not use the symbol E_0 to denote the external field as in Yeh and Berkowitz[38]), the perpendicular polarization attains a value of $p_\perp \approx 0.8$ D, as shown in Figure 4a (red profile). This signal should be compared with the dipole signal $p_\parallel \approx 0.8$ D (Figure 1c), which occurs when $E_\parallel \approx 0.015$ VÅ^{-1}, i.e., at same local fields. Note the difference between these two aforementioned profiles: $p_\perp$ reaches 80% of its new equilibrium state value in less than 20 fs (Figure 4a, red profile) and its new equilibrium state value in less than 200 fs, whereas $p_\parallel$ reaches almost the new equilibrium state in approximately 40 ps (Figure 1c, in between the two lowest blue profiles). Hence, at the same *local* electric field the signal $p_\perp$ reaches the new equilibrium state 200 times faster than it does in the parallel direction.

This dramatic difference between the dipole alignment dynamics in the perpendicular and parallel directions at equal local field appears to be constant for channel widths in the range 11−100 nm, as shown in the following. Indeed, we showed that $\epsilon = \epsilon_\perp = \epsilon_\parallel$, assuming that in the parallel direction the local field can be approximated by the external field (see the Appendix: Polarizability of Water), and neglecting the details of the interfacial dielectric profile close to the walls.[30] As explained by fitting the data with the Langevin function, these characteristics are not due to nonlinear effects. It is interesting to note that, in Figure 4a, 5−6 strong oscillations of period ∼20−30 fs are visible occurring in the first 200 fs for every field amplitude, with frequency independent of field strength and amplitude increasing with the applied field. The highest electric field 1 VÅ^{-1} shows significant oscillation amplitudes (around ∼0.3 D), while preserving the oscillation frequency. These oscillations are present also in the parallel direction, as can be seen in Figure 4b where $p_\parallel$ and $p_\perp$ are compared on the very short time scale of ∼300 fs. Figure 4b also shows that while $p_\parallel$ steadily increases (up to completing its relaxation in ∼7−10 ps if the field is low), $p_\perp$ remains constant and will conserve the value attained for $t \lesssim 30$ fs. The collective reorganization of hydrogen bonds occurring in the parallel direction (and in the homogeneous systems) manifests as the classical Debye dipolar relaxation mechanism in water. This mechanism appears to be strongly affected by the confinement in the perpendicular direction.

The equation for the dielectric relaxation[14,15,17,50] is to a first approximation given by

$$\frac{d\mathbf{p}}{dt} = \frac{\alpha\mathbf{E} - \mathbf{p}}{\tau} \tag{6}$$

where $\mathbf{p} = \mathbf{M}(t)/N_w$, τ is the dielectric relaxation time, α is the water polarizability, and $\mathbf{E}$ is the steady and spatially invariant local field. Integrating eq 6 for the parallel direction and assuming that the fluid is not polarized at t = 0, i.e., $p_\parallel$ = 0 at t = 0, gives

$$p_\parallel(t) = \alpha_\parallel E_\parallel (1 - e^{-t/\tau_\parallel}) \tag{7}$$

which when fit with the time-series of $p_\parallel(t)$ plotted in Figure 1c gives an estimate of $\tau_\parallel$ (and $\alpha_\parallel$; see the Appendix: Polarizability of Water). Figure 4c plots the dielectric relaxation time of water. In the interval $E \lesssim 0.02$ V Å^{-1}, $\tau_\parallel$ is equal to ∼8 ps for both the confined and homogeneous system, in accord with previous MD[17] and experimental results.[51,52] For every field, when the temperature increases from T = 300 to 350 K, $\tau_\parallel$ approximately halves for both the homogeneous and confined system because the higher thermal energy reduces the cohesivity of the hydrogen bond network, allowing for a faster relaxation toward the direction of the applied field. When the field amplitude increases, $\tau_\parallel$ decreases because of the higher

DOI: 10.1021/acs.langmuir.6b00791
Langmuir 2016, 32, 4765−4773

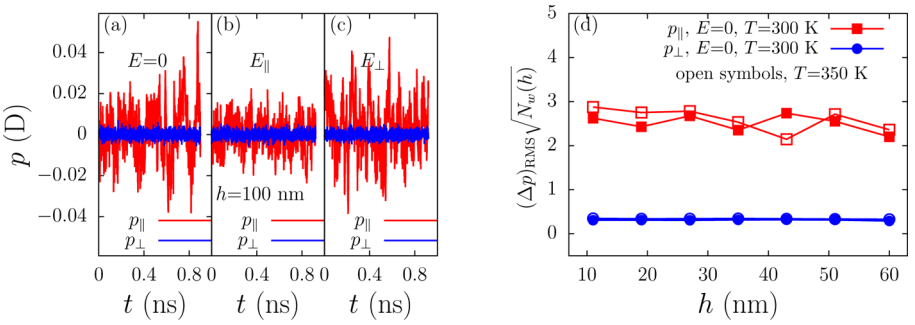

Figure 5. Polarization of confined water for channel width h = 100 nm, (a) no field, (b) parallel, and (c) perpendicular fields of magnitude E = 0.04 VÅ $^{-1}$. (d) rms fluctuations in the polarization with the channel width h.

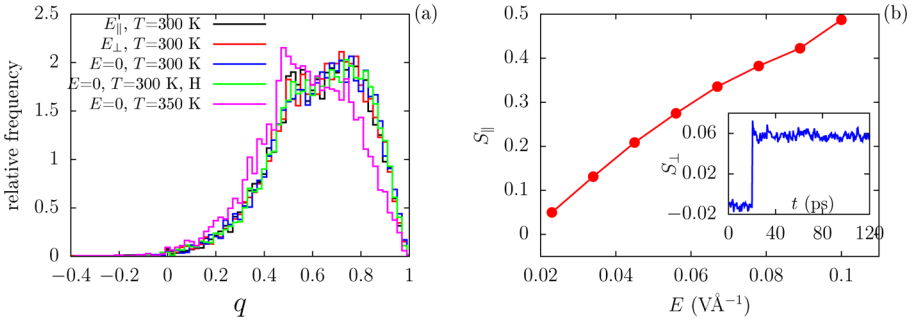

Figure 6. (a) Tetrahedral order parameter. Channel width h = 11 nm and E = 1 VÅ^{-1}. H indicates the homogeneous system. (b) Second order parameters, $S_{\parallel}$ and $S_{\perp}$, are when the field is applied in parallel and perpendicular directions to the walls.

torque exerted on the dipole. However, $\tau_{\perp}$ cannot be obtained fitting by an exponential curve, as can be seen in Figure 1d and more clearly in Figure 4a, because the signal oscillates at high frequency several times before reaching its new equilibrium state value, and its peak value is reached the first time in less than 20 fs. At zero field and T = 300 K, the perpendicular dielectric relaxation of water confined between two graphene surfaces[8] was less than approximately 200 fs and the radial dielectric relaxation in carbon nanotubes[53] was approximately 500 fs. Finally, faster perpendicular relaxation dynamics can also be observed applying a rotating electric field and measuring the phase shift between the field and the net dipole, which would be much smaller for the perpendicular direction.[15] The large difference between $\tau_{\perp}$ and $\tau_{\parallel}$ demonstrates that the physical mechanism underlying the orientational dynamics in the perpendicular direction of a confined system is different from the Debye bulk relaxation, revealing from a different perspective the existence of a fundamental anisotropy in the hydrogen bond network for confined water. We emphasize that up to the channel width h = 100 nm this difference remains unchanged. Hence, the dipoles experience almost no friction in the perpendicular alignment, revealing the presence of a confinement induced preferential route for their reorientation. It would be interesting to examine if the rotational diffusion of water has a tensorial character due to the confinement, i.e., if the measured rotational diffusion in the parallel and perpendicular direction are different. However, this will be the subject of a future investigation.

We next examine the fluctuation amplitude of the average dipole moment. Figure 5a–c shows the signals $p_{\parallel}(t)$ and $p_{\perp}(t)$ over 1 ns simulation time and for the channel width h = 100 nm at zero field, and when the field is applied in the parallel and perpendicular direction, respectively. In Figure 5a the fluctuations around the dipole moment average value are strongly damped in the perpendicular direction, in agreement with the equilibrium simulations of Zhang et al.[8] for graphene channel widths up to 30 nm. In our analysis, we quantify the amplitude of the dipole moment fluctuations by computing the root-mean-square of the fluctuations of the polarization signal

$$\Delta p_{\mathrm{rms}} = \sqrt{\frac{\sum_{i=1}^{N}(p_i - \bar{p})^2}{N}} \tag{8}$$

where $\bar{p}$ is the average dipole moment $\Sigma_{i=1}^{N} p_i/N$ over N samples and p_i is the dipole moment of the sample i. Results are summarized in Figure 5d. To avoid trivial system size effects Δp_{rms} is multiplied by $\sqrt{N_{\mathrm{w}}(h)}$, i.e., the number of water molecules for the channel width h. Data points are computed by averaging over 2000 values sampling every 500 fs for 1 ns. It is evident that the higher temperature does not substantially affect the fluctuation amplitudes of $p_{\perp}(t)$ and $p_{\parallel}(t)$. In the following, we denote the rms fluctuation amplitudes in the perpendicular direction with the symbol $\Delta p_{\perp}$ and parallel direction $\Delta p_{\parallel}$. We note that increasing h yields approximately constant parallel fluctuation amplitudes, with small differences increasing the temperature to T = 350 K. The perpendicular fluctuation amplitudes remains almost exactly constant and shows no dependence on the temperature. Moreover, results obtained with a separation of ∼10 nm are approximately equal to results taken with a channel width h = 100 nm. One would expect the rms fluctuation amplitudes of the perpendicular total dipole moment to approach that of the bulk fluid as h increases, but this is not what we observe. In fact, our attempts to quantify any dependence of the fluctuation amplitudes with h in order to extrapolate to large distances were thwarted by the flat rms trend values (Figure 5d). Perhaps the most fundamental question is exactly when is the isotropic or bulk condition $\Delta p_{\parallel}$ = $\Delta p_{\perp}$ recovered, since the flat fitting curve in Figure 5d

DOI: 10.1021/acs.langmuir.6b00791
Langmuir 2016, 32, 4765−4773

potentially extrapolates to macroscopic h sizes. The curve is so close to a flat line that as h increases no statistically meaningful fits can be made to extrapolate into the bulk, which makes a quantitative prediction impossible. Finally, we point out that applying an external electric field approximately halves the rms amplitude of the fluctuations in the parallel direction, whereas only a small effect is observed on the fluctuations in the perpendicular direction, as can be seen in Figure 5b and c, respectively.

We look at whether $\Delta p_\perp < \Delta p_\parallel$ is associated with some structural changes among the water molecules in confinement environment. Water is overall tetrahedrally coordinated,[54] a characteristic which is quantified calculating the tetrahedral order parameter[55]

$$q_i = 1 - \frac{3}{8}\sum_{j=1}^{3}\sum_{k=j+1}^{4}\left(\cos\theta_{ijk} + \frac{1}{3}\right)^2 \tag{9}$$

where j and k span the set formed by the four closest oxygen molecules to a central oxygen i and θ_{ijk} is the angle subtended by the segments joining the oxygen i and two of its four nearest neighbors j, k. The average value of q is 0 for a random system such as the ideal gas, and 1 for a perfect tetrahedral environment. For this calculation, we do not include water closer than 2 nm from the surface to avoid the large distortion of the water structure next to the interfaces.[56] Figure 6a plots the $\langle q\rangle$ histograms at zero field for the homogeneous system at T = 300 K, the graphene confined system, and the confined system at T = 350 K.

It can be seen that the tetrahedral structure of water is unchanged by the confinement, i.e. q for the confined and homogeneous system are approximately the same. The large anisotropy of dielectric relaxation times and the r.m.s. fluctuations is therefore not related to an alteration of the water tetrahedral arrangement at least in terms of the definition used. We also have verified that applying the electric fields in the range used in this work does not substantially affect the tetrahedral coefficient value. We emphasize at this point that the negligible effect of the electric field on the tetrahedral structure of water, and the correct average dipole moment alignment for every electric field amplitude, suggests that an excessive system pressure build-up, due only to molecular alignment, is unlikely. The correct dipole alignment can be seen by inspecting Figure 3c and noticing that the dielectric response is in good agreement with the theoretical prediction by Booth for the field-dependent dielectric constant of water.[38] However, a more careful study of the effect of the application of the electric field on the pressure of a confined fluid system in a NVT ensemble requires specific methods[57] and will be the subject of further investigation. Heating the confined liquid at T = 350 K, decreases the tetrahedral order compared to T = 300 K, shifting to the left the tetrahedral peak, in accord with MD[55] and experimental[58] investigations.

We examine the order parameter[59]

$$S = \frac{1}{2}\langle(3\cos^2\theta - 1)\rangle \tag{10}$$

where S = 1 for parallel, S = −1/2 for perpendicular, and S = 0 for random alignment of molecular dipoles. The angle θ is defined by $\cos\theta = \hat{\mathbf{n}}\cdot\hat{\mathbf{E}}$, where $\hat{\mathbf{E}}$ is the applied field direction and $\hat{\mathbf{n}}$ is the dipole moment direction. We have excluded the first 2 nm width fluid slabs closest to the interfaces to avoid surface induced orientation effects. As shown in Figure 6b, $S_\parallel$ increases when $E_\parallel$ increases for the larger torque exerted by the larger fields. By applying a large field, $E_\perp$ = 1 V Å^{-1}, the local field, as observed, is approximately ∼0.017 V Å^{-1}, and the order parameter reaches $S_\perp \sim 0.06$ as can be seen on the inset of Figure 6b, which depicts the time-series of $S_\perp$, comparable to $S_\parallel$ when the local field is $E_\parallel \sim 0.02$ V Å^{-1}. Hence, computations of the second order parameter of water when the local electric field for the parallel and perpendicular directions is similar, show that also the dipole ordering is similar.

CONCLUSION

In this work, we have demonstrated that confinement induces an anisotropy in the dielectric relaxation of water which extends up to at least mesoscale dimensions. We have tracked the total dipole moment of liquid water applying an electric field and observing the effect of changing the direction of the field, parallel and perpendicular to the walls, and monitoring the corresponding dipole component response. The difference found is large even for channel widths of ∼100 nm. The data strongly suggests that this anisotropy may extend much further, perhaps even to macroscopic dimensions.

We illustrated that the polarization relaxation in the perpendicular direction, when the electric field points in the confined direction, is approximately 200 times faster than the parallel dipolar response, at equal local electric fields. We conjecture that the confinement induces a preferential path on the hydrogen bond network for the dipole moments to collectively align with a perpendicular electric field, without having to overcome any significant energy barrier. The perpendicular component of the net dipole moment relaxes toward the new equilibrium state in a few femtoseconds, even for mesoscale channel sizes.

We measured the root-mean-square fluctuation amplitudes of the dipole moment, showing that in the perpendicular direction these values are 1 order of magnitude smaller than the fluctuation amplitudes of the parallel direction, and that this difference is approximately constant, hence, does not depend on the channel width, in the range 10−100 nm studied here. The results suggest that the isotropic condition, i.e., equal parallel and perpendicular root-mean-square amplitudes of fluctuations of the total dipole moment, may not be attained until macroscopic dimensions are reached. Future investigations will address the possibility of a connection between the hydrophobic forces, whose physical mechanism is still unknown,[60] and the dielectric properties of water under confinement. If the strong reduction of the fluctuation amplitudes of the total dipole moment in a confined environment corresponds to a reduction of the entropy of water, then this entropy loss may be the driving force for the hydrophobic force itself. Assuming the validity of this hypothesis, one might then suggest that hydrophobic forces are present whenever $\Delta p_\perp < \Delta p_\parallel$, and that they may extend to macroscopic dimensions.

APPENDIX: POLARIZABILITY OF WATER

The polarizability of water can be estimated using eq 7, via $\alpha_\parallel = \langle p_\parallel\rangle/E_\parallel$ obtained for $t \to \infty$. For E = 0.012 V Å^{-1}, sufficiently low to be in the linear regime (as can be seen from Figure 1c where $\tau_\parallel$ yields ∼8 ps or from Figure 2c of the text where $p_\parallel$ still linearly depends on E), we attain $\langle p_x\rangle$ = 0.55 D (Figure 1c) giving $\alpha_\parallel = 3.2 \times 10^6$ m^2 kg^{-1} eV^{-1}, in agreement with the literature.[17] From eq 1

DOI: 10.1021/acs.langmuir.6b00791
Langmuir 2016, 32, 4765−4773

$$\epsilon = 1 + \rho\alpha/\epsilon_0 \quad (11)$$

we get the dielectric constant of water $\epsilon_{\parallel} \sim 60$, close to previous published results for SPC/E model.[17]

AUTHOR INFORMATION

Corresponding Author

*E-mail: s.deluca@unsw.edu.au. Tel.: (+61) 451637539.

Author Contributions

All authors contributed substantially to the work presented in this manuscript and participated in the discussion. S.D.L. conceived the molecular dynamics experiment and wrote the paper, with input from all the authors. S.D.L. and S.K.K. performed the simulations and data analysis. S.D.L. suggested the connection between the dipolar fluctuations and the hydrophobic forces.

Notes

The authors declare no competing financial interest.

ACKNOWLEDGMENTS

Computational resources were provided by the Swinburne Supercomputer Centre, the Victorian Partnership for Advanced Computing HPC Facility and Support Services and an award under the Merit Allocation Scheme on the NCI National Facility at the Australian National University. J.S.H. wishes to acknowledge Lundbeckfonden for supporting this work as a part of Grant No. R49-A5634. The authors would thank Dr. Stefano Bernardi, Professor Debra Bernhardt, Professor Richard Sadus, and Professor Jeppe Dyre for helpful discussions of our work. The authors thank the three anonymous reviewers for the constructive and stimulating comments, which helped to improve the quality of this paper significantly.

REFERENCES

(1) Faeder, J.; Ladanyi, B. M. Molecular Dynamics Simulations of the Interior of Aqueous Reverse Micelles. *J. Phys. Chem. B* **2000**, *104*, 1033−1046.

(2) Lopez, C.; Nielsen, S.; Klein, M. L.; Moore, P. B. Hydrogen bonding structure and dynamics of water at the dimyristoylphosphatidylcholine lipid bilayer surface from a molecular dynamics simulation. *J. Phys. Chem. B* **2004**, *108*, 6603−6610.

(3) Colosi, C.; Costantini, M.; Barbetta, A.; Cametti, C.; Dentini, M. Anomalous Debye-like dielectric relaxation of water in micro-sized confined polymeric systems. *Phys. Chem. Chem. Phys.* **2013**, *15*, 20153−60.

(4) Zheng, J.; Pollack, G. Long-range forces extending from polymer-gel surfaces. *Phys. Rev. E: Stat. Phys., Plasmas, Fluids, Relat. Interdiscip. Top.* **2003**, *68*, 031408.

(5) Toney, M. F.; Howard, J. N.; Richer, J.; Borges, G. L.; Gordon, J. G.; Melroy, O. R.; Wiesler, D. G.; Yee, D.; Sorensen, L. B. Voltage-dependent ordering of water molecules at an electrode-electrolyte interface. *Nature* **1994**, *368*, 444−446.

(6) Reedijk, M. F.; Arsic, J.; Hollander, F. F. A.; de Vries, S. A.; Vlieg, E. Liquid Order at the Interface of KDP Crystals with Water: Evidence for Icelike Layers. *Phys. Rev. Lett.* **2003**, *90*, 066103.

(7) Tielrooij, K.; Paparo, D.; Piatkowski, L.; Bakker, H.; Bonn, M. Dielectric Relaxation Dynamics of Water in Model Membranes Probed by Terahertz Spectroscopy. *Biophys. J.* **2009**, *97*, 2484−2492.

(8) Zhang, C.; Gygi, F.; Galli, G. Strongly anisotropic dielectric relaxation of water at the nanoscale. *J. Phys. Chem. Lett.* **2013**, *4*, 2477−2481.

(9) von Domaros, M.; Bratko, D.; Kirchner, B.; Luzar, A. Dynamics at a Janus interface. *J. Phys. Chem. C* **2013**, *117*, 4561−4567.

(10) Singh, S. K.; Saha, A. K.; Singh, J. K. Molecular Simulation Study of Vapor- Liquid Critical Properties of a Simple Fluid in Attractive Slit Pores: Crossover from 3D to 2D. *J. Phys. Chem. B* **2010**, *114*, 4283−4292.

(11) Singh, S. K.; Sinha, A.; Deo, G.; Singh, J. K. Vapor- liquid phase coexistence, critical properties, and surface tension of confined alkanes. *J. Phys. Chem. C* **2009**, *113*, 7170−7180.

(12) Liu, Y.; Panagiotopoulos, A. Z.; Debenedetti, P. G. Finite-size scaling study of the vapor-liquid critical properties of confined fluids: Crossover from three dimensions to two dimensions. *J. Chem. Phys.* **2010**, *132*, 144107.

(13) Rasaiah, J. C.; Garde, S.; Hummer, G. Water in Nonpolar Confinement: From Nanotubes to Proteins and Beyond. *Annu. Rev. Phys. Chem.* **2008**, *59*, 713−740.

(14) Hansen, J. S.; Bruus, H.; Todd, B. D.; Daivis, P. J. Rotational and spin viscosities of water: Application to nanofluidics. *J. Chem. Phys.* **2010**, *133*, 144906−144913.

(15) De Luca, S.; Todd, B. D.; Hansen, J. S.; Daivis, P. J. Molecular dynamics study of nanoconfined water ow driven by rotating electric fields under realistic experimental conditions. *Langmuir* **2014**, *30*, 3095−109.

(16) De Luca, S.; Todd, B. D.; Hansen, J. S.; Daivis, P. J. Electropumping of water with rotating electric fields. *J. Chem. Phys.* **2013**, *138*, 154712.

(17) Bonthuis, D. J.; Horinek, D.; Bocquet, L.; Netz, R. R. Electrokinetics at aqueous interfaces without mobile charges. *Langmuir* **2010**, *26*, 12614−12625.

(18) De Luca, S.; Todd, B. D.; Hansen, J. S.; Daivis, P. J. A new and effective method for thermostatting confined fluids. *J. Chem. Phys.* **2014**, *140*, 054502.

(19) Qiu, H.; Guo, W. Electromelting of Confined Monolayer Ice. *Phys. Rev. Lett.* **2013**, *110*, 195701.

(20) Vanzo, D.; Bratko, D.; Luzar, A. Nanoconfined water under electric field at constant chemical potential undergoes electrostriction. *J. Chem. Phys.* **2014**, *140*, 074710.

(21) Srivastava, R.; Singh, J. K.; Cummings, P. T. Effect of Electric Field on Water Confined in Graphite and Mica Pores. *J. Phys. Chem. C* **2012**, *116*, 17594−17603.

(22) Neumann, M. Dielectric relaxation in water. Computer simulations with the TIP4P potential. *J. Chem. Phys.* **1986**, *85*, 1567.

(23) Senapati, S.; Chandra, A. Dielectric Constant of Water Confined in a Nanocavity. *J. Phys. Chem. B* **2001**, *105*, 5106−5109.

(24) Alper, H. E.; Levy, R. M. Computer simulations of the dielectric properties of water: Studies of the simple point charge and transferrable intermolecular potential models. *J. Chem. Phys.* **1989**, *91*, 1242−1252.

(25) Watts, R. O.; Levy, R. M. Electric polarisation of water: Monte Carlo studies. *Chem. Phys.* **1981**, *57*, 185−195.

(26) Sutmann, G. Structure formation and dynamics of water in strong external electric fields. *J. Electroanal. Chem.* **1998**, *450*, 289−302.

(27) Parez, S.; Predota, M.; Machesky, M. Dielectric Properties of Water at Rutile and Graphite Surfaces: Effect of Molecular Structure. *J. Phys. Chem. C* **2014**, *118*, 4818−4834.

(28) Hansen, J. S. Reduced dielectric response in spatially varying electric fields. *J. Chem. Phys.* **2015**, *143*, 194507.

(29) Ballenegger, V.; Hansen, J.-P. Dielectric permittivity profiles of confined polar fluids. *J. Chem. Phys.* **2005**, *122*, 114711.

(30) Bonthuis, D. J.; Gekle, S.; Netz, R. R. Dielectric profile of interfacial water and its effect on double-layer capacitance. *Phys. Rev. Lett.* **2011**, *107*, 166102.

(31) Ghoufi, A.; Szymczyk, A.; Renou, R.; Ding, M. Calculation of local dielectric permittivity of confined liquids from spatial dipolar correlations. *EPL* **2012**, *99*, 37008.

(32) Teschke, O.; Ceotto, G.; de Souza, E. Interfacial water dielectric-permittivity-profile measurements using atomic force microscopy. *Phys. Rev. E: Stat. Phys., Plasmas, Fluids, Relat. Interdiscip. Top.* **2001**, *64*, 011605.

(33) Palmer, L. S.; Cunliffe, A.; Hough, J. M. Dielectric Constant of Water Films. *Nature* **1952**, *170*, 796−796.

DOI: 10.1021/acs.langmuir.6b00791
Langmuir 2016, 32, 4765−4773

(34) Metzik, M.; Perevertaev, V.; Liopo, V.; Timoshtchenko, G.; Kiselev, A. New data on the structure and properties of thin water films on mica crystals. *J. Colloid Interface Sci.* **1973**, *43*, 662−669.
(35) Zhou, B.; Kobayashi, A.; Cui, H.-B.; Long, L.-S.; Fujimori, H.; Kobayashi, H. Anomalous dielectric behavior and thermal motion of water molecules confined in channels of porous coordination polymer crystals. *J. Am. Chem. Soc.* **2011**, *133*, 5736−5739.
(36) Badyal, Y. S.; Saboungi, M. L.; Price, D. L.; Shastri, S. D.; Haeffner, D. R.; Soper, A. K. Electron distribution in water. *J. Chem. Phys.* **2000**, *112*, 9206−9209.
(37) Werder, T.; Walther, J. H.; Jaffe, R.; Halicioglu, T.; Koumoutsakos, P. On the water-carbon interaction for use in molecular dynamics simulations of graphite and carbon nanotubes. *J. Phys. Chem. B* **2003**, *107*, 1345−1352.
(38) Yeh, I.-C.; Berkowitz, M. L. Dielectric constant of water at high electric fields: Molecular dynamics study. *J. Chem. Phys.* **1999**, *110*, 7935−7942.
(39) Shvab, I.; Sadus, R. J. Atomistic water models: Aqueous thermodynamic properties from ambient to supercritical conditions. *Fluid Phase Equilib.* **2016**, *407*, 7−30.
(40) Yeh, I.-C.; Berkowitz, M. L. Ewald summation for systems with slab geometry. *J. Chem. Phys.* **1999**, *111*, 3155−3162.
(41) Plimpton, S. Fast parallel algorithms for short-range molecular dynamics. *J. Comput. Phys.* **1995**, *117*, 1−19.
(42) Ballenegger, V. Communication: On the origin of the surface term in the Ewald formula. *J. Chem. Phys.* **2014**, *140*, 161102−161106.
(43) Ballenegger, V.; Arnold, A.; Cerda, J. J. Simulations of non-neutral slab systems with long-range electrostatic interactions in two-dimensional periodic boundary conditions. *J. Chem. Phys.* **2009**, *131*, 094107−094117.
(44) Bernardi, S.; Todd, B.; Searles, D. Thermostatting highly confined fluids. *J. Chem. Phys.* **2010**, *132*, 244706.
(45) Diallo, S. O.; Mamontov, E.; Nobuo, W.; Inagaki, S.; Fukushima, Y. Enhanced translational diffusion of confined water under electric field. *Phys. Rev. E* **2012**, *86*, 021506.
(46) Böttcher, C. J. F. *Theory of Electric Polarization: Dielectrics in static fields*, 2nd ed.; Elsevier: Amsterdam, 1993.
(47) Israelachvili, J. N. *Intermolecular and surface forces*, 3rd ed.; Academic Press: San Diego, 2011.
(48) Tanaka, M.; Sato, M. Microwave heating of water, ice, and saline solution: Molecular dynamics study. *J. Chem. Phys.* **2007**, *126*, 034509.
(49) English, N. J.; MacElroy, J. Molecular dynamics simulations of microwave heating of water. *J. Chem. Phys.* **2003**, *118*, 1589−1592.
(50) de Groot, S. R.; Mazur, P. *Non-Equilibrium Thermodynamics*; Dover: Mineola, NY, 1984.
(51) Barthel, J.; Bachhuber, K.; Buchner, R.; Hetzenauer, H. Dielectric spectra of some common solvents in the microwave region. Water and lower alcohols. *Chem. Phys. Lett.* **1990**, *165*, 369−373.
(52) Ohmine, I. Liquid Water Dynamics: Collective Motions, Fluctuation, and Relaxation. *J. Phys. Chem.* **1995**, *99*, 6767−6776.
(53) Qi, W.; Chen, J.; Yang, J.; Lei, X.; Song, B.; Fang, H. Anisotropic Dielectric Relaxation of the Water Confined in Nanotubes for Terahertz Spectroscopy Studied by Molecular Dynamics Simulations. *J. Phys. Chem. B* **2013**, *117*, 7967−7971.
(54) Bertie, J.; Lan, Z. Infrared intensities of liquids. The intensity of the OH stretching band of liquid water revisited, and the best current values of the optical constants of H2O at 25 degrees C between 15,000 and 1 cm. *Appl. Spectrosc.* **1996**, *50*, 1047−1057.
(55) Errington, J. R.; Debenedetti, P. G. Relationship between structural order and the anomalies of liquid water. *Nature* **2001**, *409*, 318−321.
(56) Bakulin, A. A.; Pshenichnikov, M. S. Reduced coupling of water molecules near the surface of reverse micelles. *Phys. Chem. Chem. Phys.* **2011**, *13*, 19355−61.
(57) Todd, B. D.; Evans, D. J.; Daivis, P. J. Pressure tensor for inhomogeneous fluids. *Phys. Rev. E: Stat. Phys., Plasmas, Fluids, Relat. Interdiscip. Top.* **1995**, *52*, 1627−1638.
(58) Strazdaite, S.; Versluis, J.; Backus, E. H. G.; Bakker, H. J. Enhanced ordering of water at hydrophobic surfaces. *J. Chem. Phys.* **2014**, *140*, 054711.
(59) Gennes, P. G. D.; Prost, J. *The Physics of Liquid Crystals*; Clarendon Press: Oxford, 1993.
(60) Donaldson, S. H., Jr; Røyne, A.; Kristiansen, K.; Rapp, M. V.; Das, S.; Gebbie, M. A.; Lee, D. W.; Stock, P.; Valtiner, M.; Israelachvili, J. Developing a general interaction potential for hydrophobic and hydrophilic interactions. *Langmuir* **2015**, *31*, 2051−2064.

NOTE ADDED AFTER ASAP PUBLICATION

This paper was published ASAP on May 3, 2016, with mistakes in the text. The corrected version was reposted on May 4, 2016.

DOI: 10.1021/acs.langmuir.6b00791
Langmuir 2016, 32, 4765−4773